Microbe sampling by mucosal dendritic cells is a discrete, MyD88-independent step in ΔinvG S. Typhimurium colitis

Siegfried Hapfelmeier,[1] Andreas J. Müller,[1] Bärbel Stecher,[1] Patrick Kaiser,[1] Manja Barthel,[1] Kathrin Endt,[1] Matthias Eberhard,[1] Riccardo Robbiani,[1] Christoph A. Jacobi,[2] Mathias Heikenwalder,[3] Carsten Kirschning,[4] Steffen Jung,[5] Thomas Stallmach,[6] Marcus Kremer,[7] and Wolf-Dietrich Hardt[1]

[1]Institute of Microbiology, D-BIOL, ETH Zürich, CH-8093 Zürich, Switzerland
[2]Universitätsklinikum Tübingen, Medizinische Klinik I, 72076 Tübingen, Germany
[3]Institute of Neuropathology and [6]Institute of Clinical Pathology, University Hospital of Zurich, CH-8091 Zürich, Switzerland
[4]Institut für Mikrobiologie, Immunologie und Hygiene, Technische Universität München, D-81675 München, Germany
[5]Department of Immunology, The Weizmann Institute of Science, 76100 Rehovot, Israel
[7]Institut für Allgemeine Pathologie und Pathologische Anatomie, Technische Universität München, D-81675 München, Germany

Intestinal dendritic cells (DCs) are believed to sample and present commensal bacteria to the gut–associated immune system to maintain immune homeostasis. How antigen sampling pathways handle intestinal pathogens remains elusive. We present a murine colitogenic *Salmonella* infection model that is highly dependent on DCs. Conditional DC depletion experiments revealed that intestinal virulence of *S.* Typhimurium SL1344 Δ*invG* mutant lacking a functional type 3 secretion system–1 (Δ*invG*) critically required DCs for invasion across the epithelium. The DC-dependency was limited to the early phase of infection when bacteria colocalized with CD11c+CX3CR1+ mucosal DCs. At later stages, the bacteria became associated with other (CD11c−CX3CR1−) lamina propria cells, DC depletion no longer attenuated the pathology, and a MyD88–dependent mucosal inflammation was initiated. Using bone marrow chimeric mice, we showed that the MyD88 signaling within hematopoietic cells, which are distinct from DCs, was required and sufficient for induction of the colitis. Moreover, MyD88-deficient DCs supported transepithelial uptake of the bacteria and the induction of MyD88–dependent colitis. These results establish that pathogen sampling by DCs is a discrete, and MyD88-independent, step during the initiation of a mucosal innate immune response to bacterial infection in vivo.

CORRESPONDENCE
Wolf-Dietrich Hardt:
hardt@micro.biol.ethz.ch

Abbreviations used: Δ*invG, S.*
Typhimurium SL1344 Δ*invG*
mutant lacking a functional
TTSS-1; DTX, diphtheria toxin;
DTR, DTX receptor; EGFP,
enhanced GFP; HE, hematoxylin
and eosin; MAMP, microbe
associated molecular pattern;
mLN, mesenteric lymph node;
PP, Peyer's patch; SPF, specific
pathogen–free; *S.* Typhimurium,
Salmonella enterica subspecies 1
serovar Typhimurium; TLR,
Toll-like receptor; TTSS-1, type 3
secretion system-1; TTSS-2,
type 3 secretion system-2.

The mammalian intestine is inhabited by a dense bacterial microflora, which interacts with the intestinal mucosa in a mutually beneficial way (1). Physical, chemical, and immunological barriers of the intestinal mucosa restrict bacterial tissue invasion. However, the intestinal immune system employs M cells and intercalating DCs for transepithelial sampling of live microbes (2–6). We do not fully understand these microbial sampling pathways, in particular, whether they can recognize or avoid harmful pathogenic microorganisms. Using the model pathogen *Salmonella enterica* subspecies 1 serovar Typhimurium (*S.* Typhimurium), we have ex-

plored both the role of mucosal DCs in pathogen sampling, and the involvement of TLR–MyD88–mediated pathogen recognition by these cells in acute infection.

S. Typhimurium is a Gram-negative entero-pathogenic bacterium causing large numbers of diarrheal infections worldwide. After oral infection, *S.* Typhimurium interacts with the intestinal mucosa, invades the mucosal tissue, and triggers pronounced inflammation. This mucosal infection can be studied in calves (7, 8) and in the streptomycin-pretreated mouse model (9). In this mouse model, oral antibiotic pretreatment transiently suppresses the bacterial microflora (10). This allows efficient gut colonization by *S.* Typhimurium and triggering of intestinal inflammation, characterized by broad epithelial

lesions and an infiltrate rich in polymorphonuclear leukocytes (PMN) in the cecum and colon (9). Likewise, in humans, antibiotic treatment represents a risk factor for enteric *S*. Typhimurium infection (11). The comparable histopathology (9, 12, 13), the induction of analogous cytokine responses (14, 15) (unpublished data) and the involvement of identical *Salmonella* virulence factors required for inducing inflammation (16) corroborate that mucosal inflammation in the streptomycin–pretreated mouse model, calves, and the human disease is driven by the same pathogenetic mechanisms (16, 17).

S. Typhimurium uses two discrete pathways in parallel for entering the mucosal tissue and triggering inflammation (Fig. 1). These two pathways differ by their requirement for two main *Salmonella* virulence factors, the type 3 secretion system–1 (TTSS–1) and –2 (Fig. 1) (16), as follows. (a) The "classical" pathway: this pathway requires TTSS–1. *S*. Typhimurium mutants lacking TTSS–2 can still use TTSS–1 to invade epithelial cells and trigger early proinflammatory cytokine release, but they are severely attenuated at later stages (Fig. 1, left) (18–21). (b) The "alternative" pathway: this pathway for triggering enterocolitis requires TTSS–2. It is used by TTSS–1–deficient mutants such as the *S*. Typhimurium SL1344 Δ*invG* mutant lacking a functional TTSS–1 (termed Δ*invG* hereafter). Δ*invG* can breach the gut epithelium (20), but the mechanism of its transepithelial transport is still enigmatic. It may involve (i) "villous M-cells," (ii) paracellular translocation, or (iii) antigen-sampling DCs (Fig. 1, right) (5, 6, 22). In the lamina propria, Δ*invG* employs TTSS–2 to replicate in CD11b⁺CD11c⁻ monocytes and triggers inflammation by day 3 after infection (Fig. 1, right) (18–20, 23). This "slow" induction of colitis by Δ*invG* requires MyD88 (20), which is a key adaptor protein linking Toll-like receptors (TLRs) to the expression of proinflammatory cytokines (24).

To elicit full-blown inflammation, the TTSS–1 and –2 secretion systems are both required, and TTSS–1⁻TTSS–2⁻ double mutants are avirulent (18–20).

In this study, we analyzed the alternative pathway of *Salmonella* enterocolitis in vivo using Δ*invG S*. Typhimurium. We specifically focused on the mechanism of transepithelial sampling and the role of mucosal DCs in the induction of inflammation. DCs were found to mediate transepithelial transport of Δ*invG* into the cecal mucosa, whereas MyD88-dependent mucosal inflammation was triggered in a discrete, subsequent step. This assigns a key step in the intestinal pathogenicity of *S*. Typhimurium to DCs and defines the role of DCs in pathogen sampling by the large intestinal mucosa.

RESULTS

Specificity of DC depletion in the large intestinal mucosa

We studied the role of DCs in *Salmonella*-induced enterocolitis (Fig. 1) by means of conditional DC depletion experiments. The transgenic mouse line DTR[tg] (25) (see Materials and methods) expresses a human diphtheria toxin (DTX) receptor (DTR)/enhanced GFP (EGFP) fusion protein under the control of the CD11c promoter (Fig. S1 A, available at http://www.jem.org/cgi/content/full/jem.20070633/DC1). Hence,
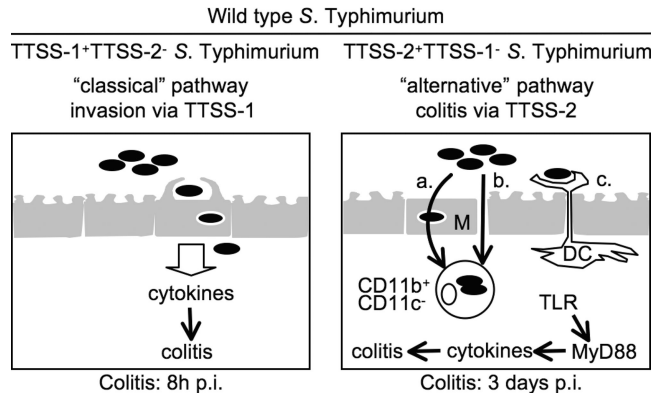

Figure 1. The *Salmonella* virulence factors TTSS–1 and –2 target two discrete pathways to induce colitis. (left) Classical pathway. TTSS-1–mediated epithelium invasion and triggering of cytokines. MyD88 is not required. (right) Alternative pathway. Mutants lacking a functional TTSS-1 (e.g., Δ*invG*) also translocate across epithelia by an unknown mechanism that could involve (a) M cell–mediated transcytosis, (b) paracellular translocation, or (c) DC-mediated luminal sampling. 3 d after infection, Δ*invG* resides in CD11b⁺CD11c⁻ lamina propria cells and induces colitis in a MyD88-dependent way. WT *S*. Typhimurium uses both pathways, and TTSS-1⁻TTSS-2⁻ double mutants are avirulent.

DTX injection allows rapid conditional depletion of DCs from organs of the immune system and the ileal part of the intestine (25–28). 12 h after DTX injection, CD11c⁺CD11b⁺ DCs were also efficiently depleted from the large intestine, as shown by immunohistology of the cecal (Fig. 2, A and B, and Fig. S1 B) and colonic mucosa (unpublished data) and FACS analysis of the large intestinal lamina propria (Fig. 2 C). This was confirmed by fluorescence microscopy analysis of DTR[tg] CX3CR1[gfp/+] double transgenic mice, which harbor brightly fluorescent mucosal DCs (Fig. 2 D) (5, 28). In contrast to the DCs, the total numbers of CD11b⁺, MOMA-1⁺, CD68⁺ (macrophage markers), NK1.1⁺ (natural killer cells; unpublished data), and CD3⁺ cells (T cells) in the cecal lamina propria were unaffected (Fig. 2, A and B, and Fig. S1 B). Immunohistochemical staining of the macrophage marker F4/80 was reduced at 12 h after DTX injection. Similar changes in F4/80 marker staining were previously described in the spleens of DTX–injected DTR[tg] mice, and attributed primarily to transient marker down-regulation (26). In addition, some CD11c^{int}CD11b⁺ cells (which may include F4/80⁺ "inflammatory" DCs) (29) were co-depleted (Fig. 2 C; see also Fig. 4 C). In conclusion, the large intestinal mucosa of DTX–injected DTR[tg] mice became depleted of DCs (i.e., CD11c⁺CD11b⁺CX3CR1⁺ cells), but for the most part retained other CD11b⁺ myeloid cell types and lymphocytes (including B cells, T cells, and NK1.1⁺ NK cells).

In mesenteric LNs (mLNs) and spleen, the DC depletion induced a distinct set of side effects. In the spleen, a CD-11c^{int}CD11b⁺ population increased (Fig. S2 A, available at http://www.jem.org/cgi/content/full/jem.20070633/DC1), whereas specific macrophage populations (marginal zone macrophages; ERTR-9⁺ and MOMA-1⁺; Fig. S2, A and C) and a CD11c^{int}GFP⁺ population (Fig. S2, A and B) were ablated.
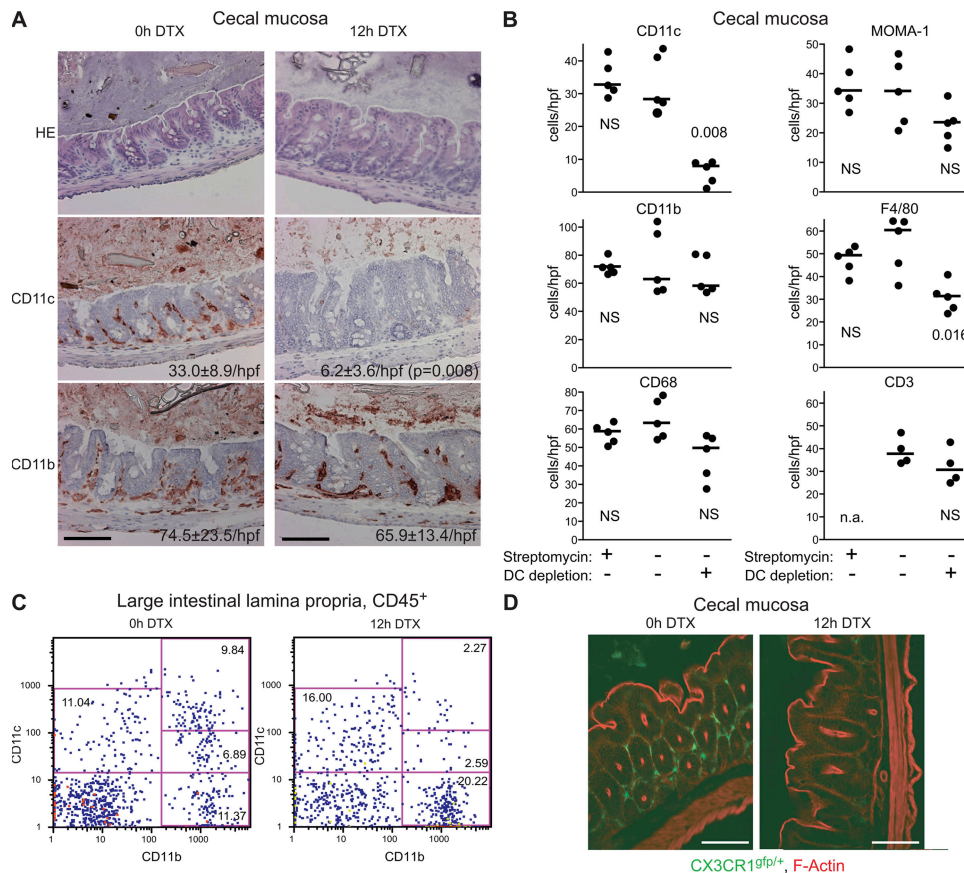
Figure 2. Conditional depletion of CD11c+ DCs from the cecal mucosa. DTR[tg] mice were analyzed before (0 h DTX) and 12 h after (12 h DTX) DTX injection (100 ng/25 g body weight i.p.). (A) Cecal tissue sections stained with HE or immunostained for CD11c or CD11b. Quantitative information was taken from (B; mean ± the SD); additional markers and time points are shown in Fig. S1 B. (B) Effects of streptomycin pretreatment and DC depletion on mucosal cell populations. CD11c+, CD11b+, CD68+, MOMA-1+, F4/80+, and CD3+ cells, stained by immunohistochemistry, were enumerated in ≥4 randomly selected high power fields of the cecal tissue from 3 independent mice. Mice were pretreated with streptomycin, and DCs were depleted as indicated. n.a., not analyzed. (C) FACS analysis of large intestinal lamina propria cells (gated on CD45+ monocytes) confirmed efficient depletion of CD11c+CD11b+ DCs. The results were confirmed in two additional, independent experiments (not depicted). (D) DC depletion in DTR[tg] CX3CR1[gfp/+] double-heterozygous mice. Green (GFP), CX3CR1+ DCs; red, actin. Bars, 100 μm. Fig. S1 is available at http://www.jem.org/cgi/content/full/jem.20070633/DC1.

The depletion of marginal zone macrophages and activated T cells has been shown previously (25, 26). However, our earlier work on LTβ receptor knockout mice and lymphopenic (RAG) mice had demonstrated that similar alterations in follicular cell populations, complete lack of intestinal follicular structures, or T and B cell deficiency do not affect the colitis induced by *S.* Typhimurium (20).

In conclusion, DCs are effectively depleted from the large intestinal mucosa in DTX-injected DTR[tg] mice with marginal effects on other cell populations known to be involved in colitis induction.

Δ*invG*-induced colitis is diminished in DC-depleted DTR[tg] mice

If Δ*invG* requires DCs for breaching the intestinal epithelium, consequences of DC depletion for lamina propria colonization, induction of colitis, and spread to mLN or systemic sites would be expected. To test this hypothesis, streptomycin-pretreated mice were infected for 3 d with Δ*invG* (Fig. 3).

Intestinal histopathology and bacterial colonization were compared between DC-depleted DTR[tg] mice, untreated DTR[tg] mice, and nontransgenic littermate controls. Neither DTX treatment by itself nor the transgene itself affected the induction of colitis or systemic dissemination (Fig. 3, A–F; see DTX-treated WT mice and nontreated DTR[tg] mice). In contrast, DC depletion in DTR[tg] mice abolished the Δ*invG* colitis (Fig. 3, A and F). This was not attributable to reduced colonization of the cecal lumen (Fig. 3 B). Furthermore, DC depletion reduced the Δ*invG* spread to mLN, spleen, and liver by >100-fold (P < 0.05; Fig. 3, C–E). This indicated that DCs are required for the initiation of acute colitis and for the initiation of systemic infection by Δ*invG*.

Effect of DC depletion on WT *S.* Typhimurium infection

Control infections were performed with WT *S.* Typhimurium (SL1344; TTSS-1+TTSS-2+). WT *S.* Typhimurium can translocate across the intestinal epithelium, and it causes colitis via the alternative and the classical pathways. In the latter case,
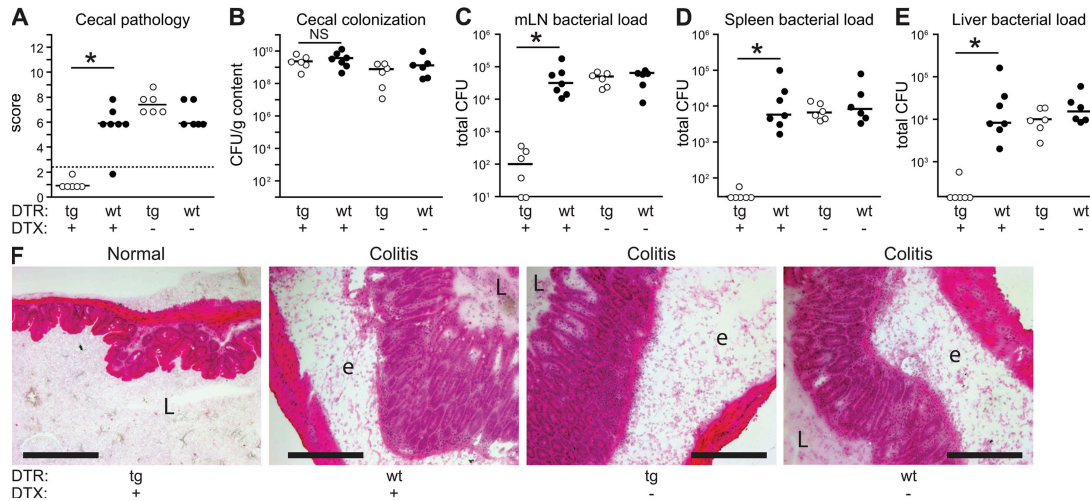
Figure 3. **The virulence of ΔinvG is diminished in DC–depleted mice.** DTR[tg] (tg, open circles) and WT littermates (WT, filled circles) were pretreated with streptomycin, injected with DTX as indicated, and infected with ΔinvG (5 × 10^{7} CFU by gavage; n = 6–7 mice/group). Cecal pathology scores (A), cecal luminal colonization (B), and bacterial loads in mLNs (C), spleens (D), and livers (E) were determined 3 d after infection. The y origin of every graph represents the detection limit. Dashed line, border between pathology score values observed in normal mice versus infected animals; *, statistically significant (P < 0.05); NS, nonsignificant (P ≥ 0.05). (F) HE-stained cryosections from representative mice of each experimental group. L, cecum lumen; e, submucosal edema. Bar, 200 μm.

the pathogen penetrates the epithelium via TTSS-1 (Fig. 1, left) (18–20). As expected, mucosal inflammation and PMN infiltration induced by WT *S.* Typhimurium were barely affected by DC depletion (Fig. 4, A and B). Immunohistochemistry and FACS analyses verified that CD11c⁺CD11b⁺ DCs and CD11c^{int}CD11b⁺ monocytes were ablated in the DC-depleted mice, whereas inflammatory infiltrates of PMN and CD11b⁺ or CD68⁺ phagocyte populations remained unchanged (Fig. 4, A [second graph], B, C). Thus, both steps of the classical pathway for colitis induction by *S.* Typhimurium, i.e., tissue invasion via TTSS-1 and induction of inflammation, are DC independent. In contrast, DC depletion specifically interfered with the alternative pathway (Fig. 3).

The spread of WT *S.* Typhimurium to the mesenteric lymph nodes was slightly delayed in the DC-depleted mice (Fig. 4 A, compare 12 and 48 h after infection). This demonstrates a partial role of DCs in early translocation of WT *S.* Typhimurium, and is in line with published data showing that, 1 d after gavage, WT bacteria can be grown from FACS-sorted mesenteric DCs and macrophages (30). However, by 48 h after infection, bacterial loads became equivalent in the mLNs of DC-depleted mice and the nondepleted controls. Furthermore, we could show that the systemic spread of the bacteria does not affect the mucosal infection (see below; Fig. S3, available at http://www.jem.org/cgi/content/full/jem.20070633/DC1), indicating that the variability of systemic loads should not compromise our analysis of the role of DCs in ΔinvG colitis.

DC depletion abrogates transepithelial translocation of ΔinvG

DC depletion could cripple ΔinvG–induced colitis via different mechanisms, such as disruption of transepithelial transport and/or elimination of DC-derived proinflammatory signals.

If DCs are needed for transepithelial transport of ΔinvG, DC depletion should reduce the rate of lamina propria colonization. To test this hypothesis, we have compared the time courses of lamina propria colonization and mucosal inflammation in DC-depleted mice and nondepleted controls (Fig. 5). In this experiment, the ΔinvG bacteria harbored a GFP reporter plasmid that allows in situ detection of intracellular *Salmonellae* by fluorescence microscopy without diminishing virulence (pM973) (20). In DC-depleted mice, the colonization of the lamina propria was strongly reduced (Fig. 5 D; day 2 and 3 after infection). Cecal inflammation and the spread to the mLN was also diminished in these animals (Fig. 5, A and C). Thus, CD11c⁺ DCs are critically important during an early step of the pathogen–host interaction, i.e., transepithelial translocation of ΔinvG into the lamina propria.

In a control experiment, mice were infected by simultaneous gavage and i.p. injection with differentially labeled ΔinvG strains (Fig. S3). The bacteria that were injected i.p. could be recovered in high numbers from systemic sites 3 d after infection in DC-depleted mice and nondepleted mice alike. Nevertheless, the bacteria of the systemic inoculum remained absent from the lamina propria (Fig. S3). This indicated that lamina propria colonization and concomitant inflammation were the result of local epithelial translocation rather than systemic-to-peripheral spread.

In conclusion, mucosal DCs are required for local epithelial traversal of ΔinvG, and this is a prerequisite for colonization of the lamina propria and induction of colitis.

DCs are required only during the initial phase of ΔinvG infection

Oral infection with ΔinvG is a multistep process that requires ∼72 h before the onset of overt colitis. The preceding
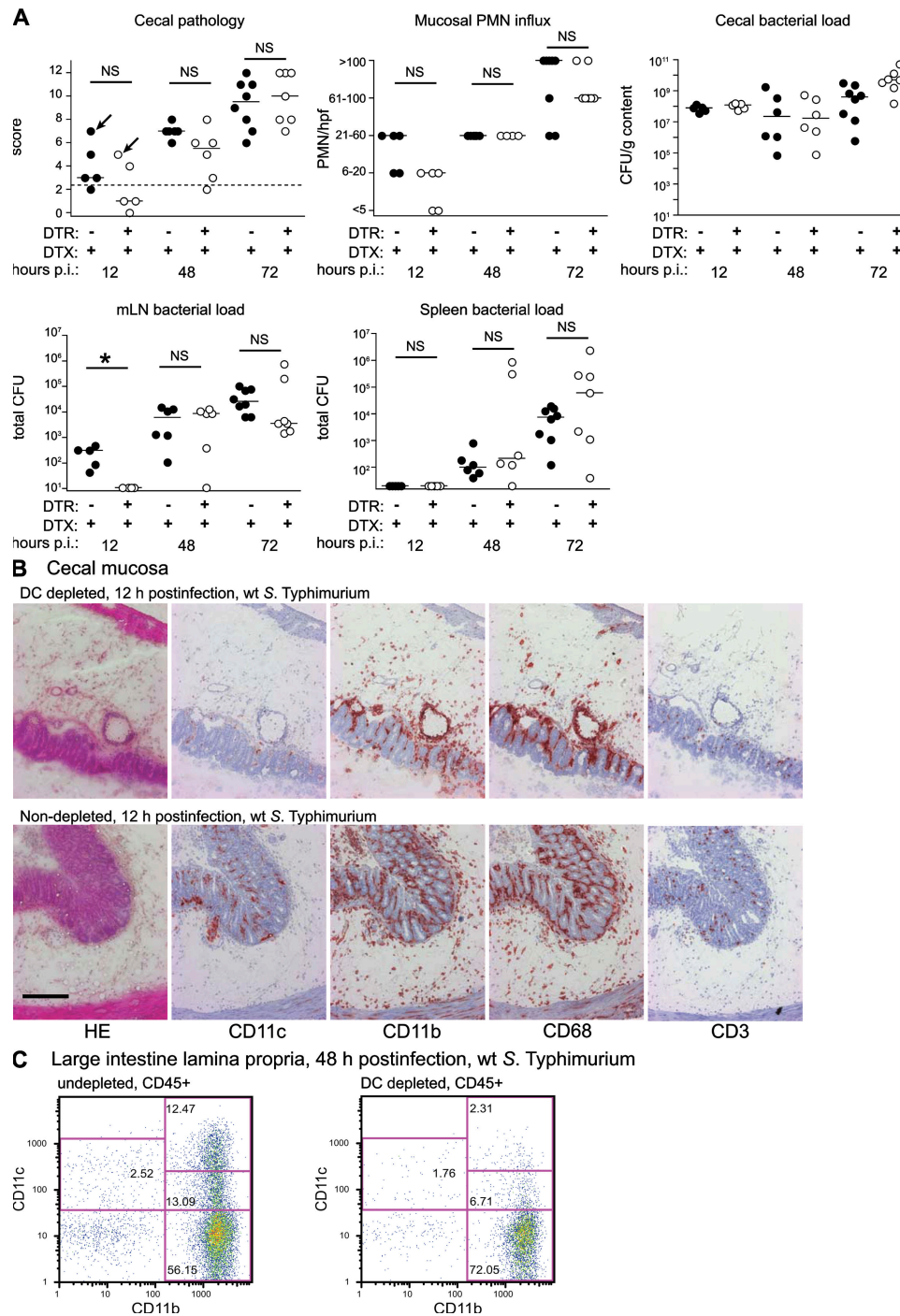
Figure 4. WT *S.* Typhimurium is also virulent in mice depleted of DCs. DTR[tg] (open circles; *n* = 5–7) mice or WT littermates (filled circles; *n* = 5–8) were pretreated with streptomycin, injected with DTX and infected with WT *S.* Typhimurium (SL1344; 5 × 10^{7} CFU by gavage). At the indicated times after infection (p.i.), the animals were killed, and tissue samples were cryoembedded and analyzed. (A) Cecal pathology scores, PMN-infiltration, luminal cecal colonization levels, and bacterial loads in mLNs and spleens. The y origin of every graph represents the detection limit. Dashed line, border between pathology score values observed in normal mice versus infected animals; *, statistically significant (P < 0.05); NS, nonsignificant (P ≥ 0.05). Arrows indicate individuals chosen for analysis in B and C. (B) Immunohistochemical analysis of cecal tissue from DC-depleted and nondepleted mice. Tissues from mice (12 h after infection; WT *S.* Typhimurium) were stained with HE or antibodies directed against CD11c, CD11b, CD68, and CD3. Bar, 200 μm. (C) FACS analysis of lamina propria cells. Large intestinal tissue cells from DC-depleted and nondepleted mice (48 h after infection; WT *S.* Typhimurium) were stained with antibodies against CD45.2, CD11c, and CD11b. Cells were gated on the CD45+ monocyte population and analyzed for CD11c and CD11b surface marker expression. The results from B and C were confirmed in two additional independent experiments (not depicted).
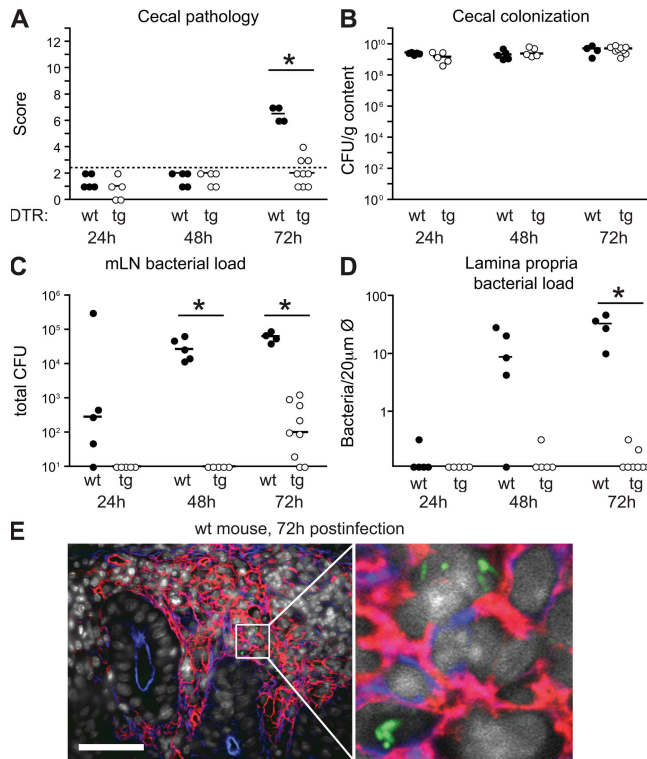
Figure 5. DC depletion abolishes lamina propria colonization by Δ*invG*. DTR[tg] (open circles) or WT littermate controls (filled circles) were pretreated with streptomycin, injected with DTX, and infected with Δ*invG*(pM973) (5 × 10^{7} CFU by gavage). 24 h (n = 5 [DTR[tg]]; n = 5 [WT]), 48 h (n = 5 [DTR[tg]]; n = 5 [WT]), and 72 h after infection (n = 9 [DTR[tg]]; n = 4 [WT]), we determined cecal pathology scores (A), luminal cecal colonization levels (B), and bacterial loads in mLNs (C). (D) Loads of intracellular bacteria in the lamina propria were determined by fluorescence microscopy (see Materials and methods). The y origin of every graph represents the detection limit. Dashed line, border between pathology score values observed in normal mice versus infected animals; *, statistically significant (P < 0.05). (E) GFP-expressing bacteria (green) in the lamina propria (CD54+, red) of a WT littermate control mouse at 3 d after infection are mostly located within inflammatory foci. To visualize GFP-expressing intracellular bacteria (green) 20 μm cryosections were stained with anti-CD54/ICAM-1 monoclonal antibody (red: lamina propria), A647-conjugated phalloidin (blue; actin), and DAPI (gray; nuclei). Bar, 50 μm.

experiments did not reveal whether the essential role of DCs is restricted to transepithelial transport or rather extends to the subsequent phases of the disease. This was analyzed via "delayed DC depletion" experiments in DTR[tg] mice. DCs were removed using a modified depletion schedule (DTX injection at 6 or 30 h after infection), which led to DC depletion at ∼18 and 42 h after infection, respectively. In the control groups, DCs were depleted for the entire course of the infection or remained undepleted. All four groups were pretreated with streptomycin, infected with Δ*invG* (5 × 10^{7} CFU by gavage), and analyzed 3 d after infection. Delayed DC depletion neither abrogated colitis nor prevented bacterial colonization of the lamina propria (Fig. 6 A). Notably, the characteristic histopathological features (i.e., inflammatory focus formation and

crypt loss) (20) of Δ*invG*–induced colitis and the infiltration of these lesions by CD11b^{+}, CD68^{+}, or Gr-1^{+} phagocytes were identical in delayed DC-depleted animals and nondepleted mice (Fig. 6 B).

In conclusion, the critical role of DCs is limited to the first hours of the pathogen–host interaction. This includes bacterial sampling and possibly early steps of DC maturation/activation. Downstream of this, CD11c^{+} DCs may still contribute to initiating adaptive immune responses, but subsequent steps toward colitis and systemic infection can proceed in absence of these cells.

Δ*invG* is localized within CD11c^{high}CX3CR1^{high} mucosal DCs at early stages, and in CD11c^{−}CX3CR1^{−} lamina propria cells at later stages of the infection

Our data indicated that DCs are critically important for transepithelial transport of Δ*invG* during the first phase of the infection. Thus, direct sampling of luminal pathogens by mucosal DCs might be involved, e.g., via extensions penetrating through the cecal epithelium. However, we and others have not observed this type of DC extension in the large intestinal mucosa (Fig. S4, available at http://www.jem.org/cgi/content/full/jem.20070633/DC1) (4, 5). If, in fact, cecal/colonic DC dendrites are formed, their low frequency and/or their too short lifetime may prevent unequivocal detection by fluorescence microscopy. However, detection of bacteria within lamina propria DCs may well be possible and provide evidence for a direct luminal uptake mechanism. Therefore, we analyzed the physical association of DsRed-labeled Δ*invG* with cecal CD11c^{+}CX3CR1^{+} DCs in situ. CD11c-EYFP transgenic mice, which express a bright EYFP reporter construct under control of the CD11c promoter in the mucosal DCs (Fig. 7, A, C, and D) (31), and CX3CR1[gfp/+] mice (Fig. 7, B and E) were pretreated with streptomycin, infected with Δ*invG*(pDsRed), and analyzed at days 1, 2, and 3 after infection. 1 d after infection, only very few bacteria were detected within the lamina propria, but they exclusively resided within DCs (dendritic cell shape and high expression levels of the CD11c-YFP or CX3CR1-EGFP [Fig. 7, A and B]). In line with the data presented in Fig. 5 D, the bacterial load in the lamina propria had increased by 2 d after infection, and 58 ± 18% (mean ± SD) of these bacteria resided within DCs (Fig. 7, A and B). Our earlier work had shown that the fraction of lamina propria–localized Δ*invG* residing in CD11c^{+} DCs further declines to ∼5–10% at 3 d after infection. (20). This was verified in the CX3CR1[GFP/+] mice (Fig. 7 B). These data provide clear evidence for a direct physical pathogen–DC interaction during the early phase of the Δ*invG* infection.

The bacterial cells localized in non-DCs 3 d after infection could be derived from either continuous transepithelial uptake or from a two-step process of DC-mediated uptake, followed by proliferation in the lamina propria. We hypothesized that bacteria derived from relatively few DC sampling events persist and proliferate locally in the lamina propria. This eventually causes the abscess-like inflammatory lesions (only ∼20–50 total per cecum) that contain most of the lamina propria-localized
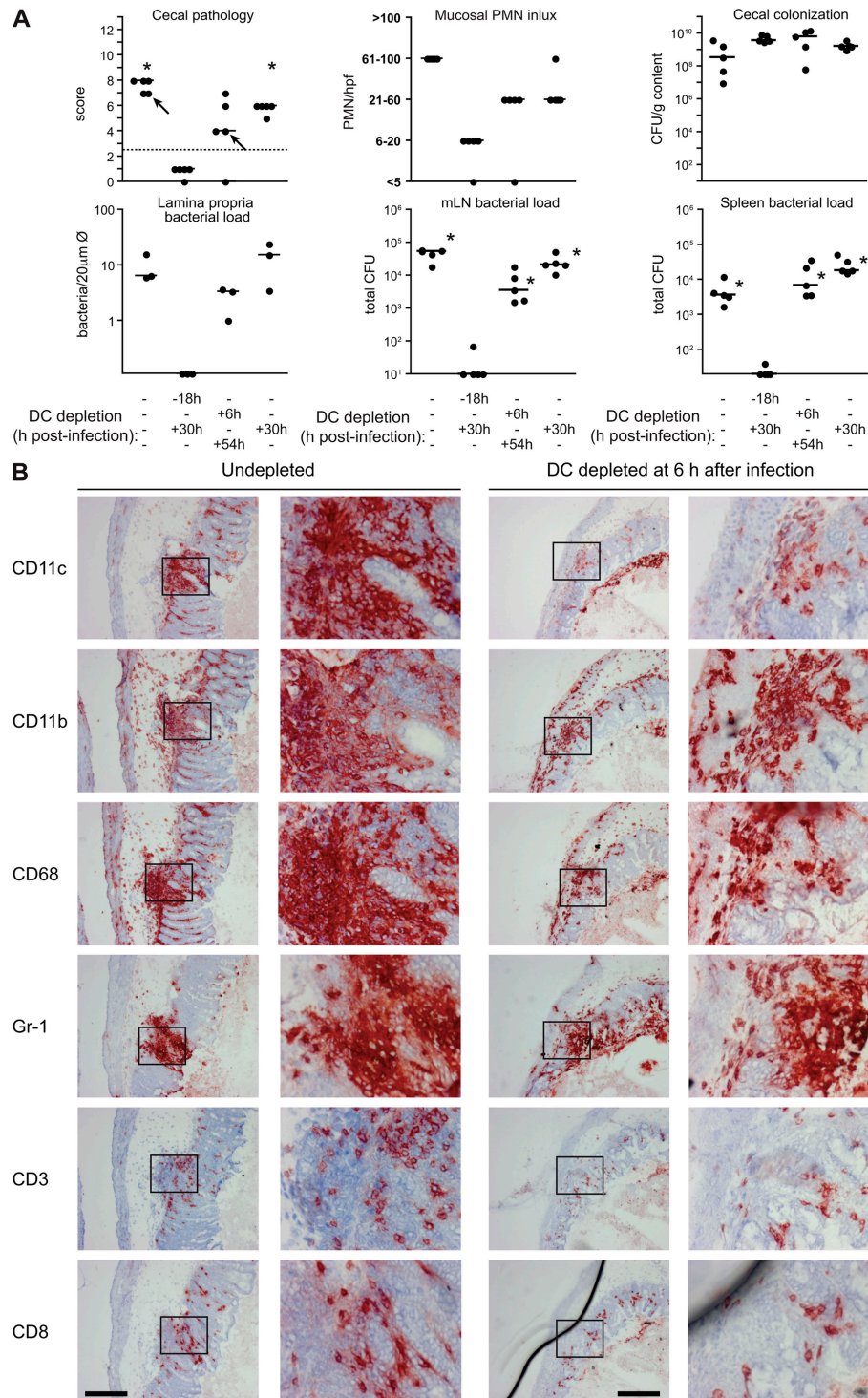
Figure 6.   DCs are required only during the initial phase of the Δ*invG* infection. 4 groups of DTR[tg] (*n* = 5) mice were pretreated with streptomycin, injected with DTX at the indicated time points, and infected with Δ*invG* (*n* = 2) or Δ*invG*(pM973) (*n* = 3; 5 × 10^{7} CFU by gavage). (A) Cecal pathology scores, PMN infiltration, bacterial loads in the cecal lumen, lamina propria (*n* = 3 expressing GFP), mLNs, and spleens at 3 d after infection. The y origin of every graph represents the detection limit. Dashed line, border between pathology score values observed in normal mice versus infected animals; statistical comparisons with the negative control (DC-depletion according to the standard protocol) are shown: asterisk, statistically significant (P < 0.05). Arrows: individuals chosen for analysis in (B). (B) Immunohistochemical analysis of cecal tissue from DC-depleted and nondepleted mice. Tissues were stained with HE or antibodies against CD11c, CD11b, CD68, Gr-1, CD3, and CD8 (see Materials and methods). The results were confirmed in an additional, independent experiment (not depicted). Note: the delayed DC-depleted individual had a smaller pathology score than the control animal (A, first panel), explaining the difference in size (at similar cellular composition) of the two inflammatory foci shown. Bars, 200 μm.
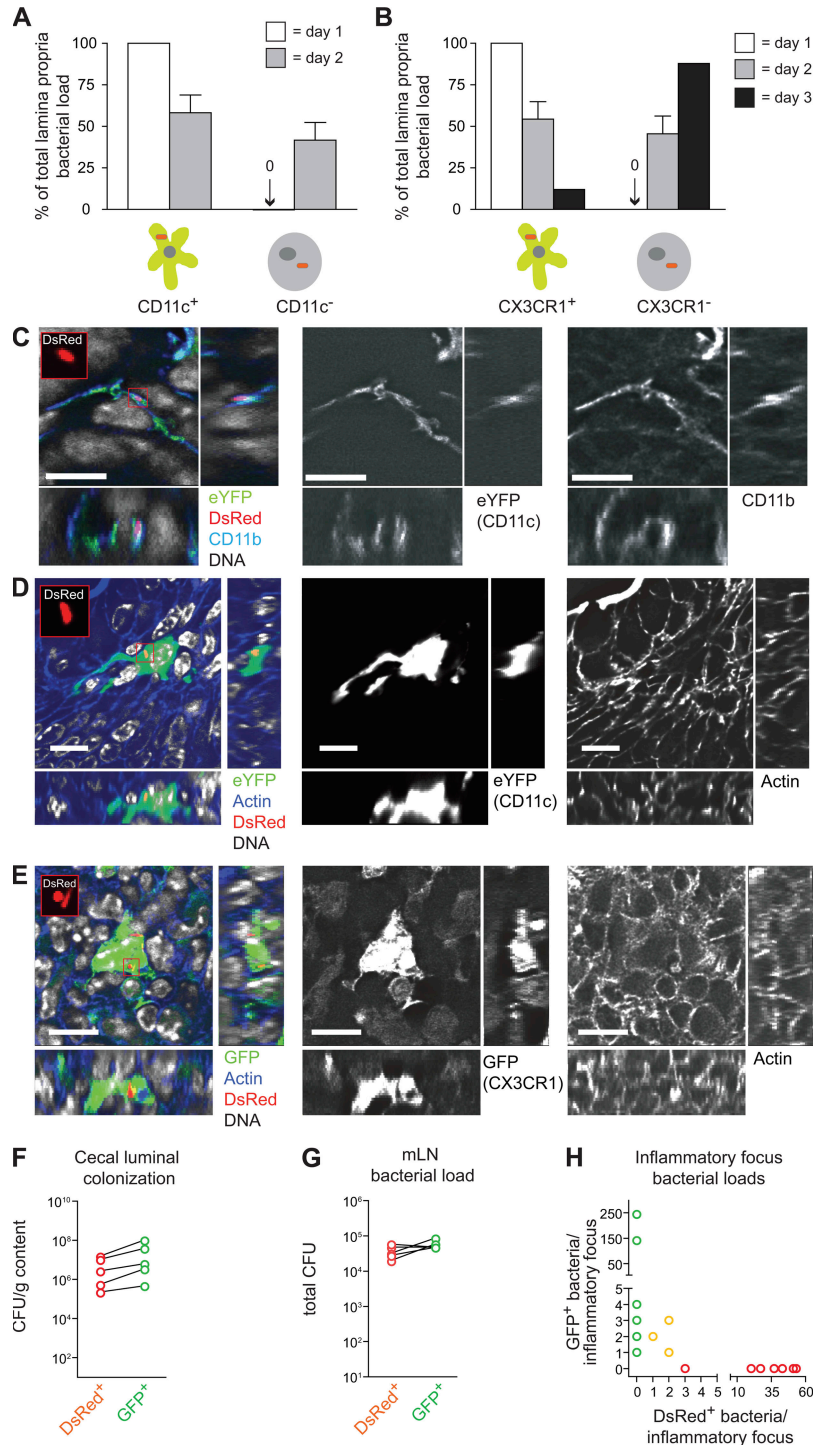
Figure 7. Changes in the *Salmonella*–DC association and evidence for a bottleneck restricting lamina propria colonization by Δ*invG*. (A and B) Groups of *n* = 3 CD11c-EYFP (A) or CX3CR1[gfp/+] (B) transgenic mice were pretreated with streptomycin, infected with Δ*invG*(pDsRed) (5×10^7 CFU by gavage) and killed at 24 and 48 h (or 72 h) after infection, respectively. 20-μm cryosections of cecal tissue were counterstained with DAPI (DNA) and A647-phalloidin (F-actin), and the percentage of DsRed[+] bacteria colocalizing with EYFP[+] (A) or GFP[+] (B) DCs or EYFP[−]/GFP[−] lamina propria cells was determined. DsRed expression was detected in bacteria located in the mucosal tissue, but not in the gut lumen. (A and B) 1 d after infection, a total of 5 (A) or 3 (B) DsRed-expressing lamina propria bacteria were detected in 15 nonserial sections. Error bars show the mean ± the SD. (C) Δ*invG*(pDsRed) localization in CD11c^{+}CD11b^{+} DCs. A 20-μm-thick cecal tissue section of a mouse from (A; 2 d after infection) showing a CD11c/EYFP^{+} cell (green) was stained with DAPI (DNA, gray) and an anti-CD11b antibody (CD11b, blue) and imaged confocally. (D and E) Δ*invG*(pDsRed) localization in CD11c^{+} or CX3CR1^{+} DCs. 20-μm-thick cecal tissue sections of mice from (A and B; 2 d after infection) showing a CD11c/EYFP^{+} (D; green) or a CX3CR1/GFP[+] cell (E; green) were stained with DAPI (DNA, gray) and A647-phalloidin (F-actin, blue) and imaged confocally. Bars, 10 μm. (F–H) Co-infection with DsRed- and GFP-expressing bacteria.

bacteria at day 3 after infection. We found strong evidence for such a two-step process in a co-infection experiment using a 1:1 mixture of GFP- and DsRed-expressing Δ*invG* bacteria. In line with our hypothesis, most mucosal inflammatory lesions at day 3 contained either GFP+ or DsRed+ (i.e., clonal) bacterial populations (Fig. 7, F–H). Thus, most inflammatory foci were populated by the progeny of a single bacterium. A narrow "bottleneck" seemed to be inflicted on Δ*invG*, possibly by bactericidal intestinal macrophages (30, 32), limited numbers of DC-sampling events, or killing during transepithelial up-take. Furthermore, because bacteria of clonal origin resided in multiple host cells, they clearly had been propagated from the cell responsible for transepithelial uptake (DCs) to other lamina propria host cells (ultimately, CD11b+CD11c− cells).

In conclusion, our data clearly demonstrate that colonization of the large intestinal lamina propria by Δ*invG* is a multistep process of DC-dependent epithelial translocation, followed by bacterial proliferation in the lamina propria, and bacterial transfer between different host cells.

MyD88 signaling in BM–derived leukocytes is required and sufficient for induction of colitis by Δ*invG*

As shown above, mucosal DCs are critical for initiating colonization of the cecal lamina propria by Δ*invG*. Earlier work had demonstrated that Δ*invG* requires MyD88 for triggering colitis (20). DCs express most of the known TLRs and require MyD88 for TLR ligand-induced production of pro-inflammatory/T helper type 1 cell polarizing cytokines, such as TNFα, IL-6, and IL-12p40 (33, 34; for review see [35]). We hypothesized that the requirement for MyD88 signaling might reside within the same mucosal DCs that are mediating translocation of Δ*invG* into the lamina propria.

Before testing this hypothesis, we needed to determine whether MyD88 signaling was required in BM-derived leukocytes (including DCs), non–BM-derived cells (i.e., epithelial or stromal cells), or both. Radiation BM chimera were created by reconstitution of γ-irradiated WT (Ly5.1) and MyD88−/− (Ly5.2) mice with MyD88−/− (Ly5.2) and WT (Ly5.1) BM, respectively. Reconstitution efficiencies were >95%, as determined by postmortem FACS staining for Ly5.1 and Ly5.2 on CD11c+ DCs and B220+ B cells from spleens and mLNs (unpublished data). 8 wk after irradiation, the BM chimeras were studied in Δ*invG* infection experiments. MyD88−/−, MyD88+/− littermates, and WT C57BL/6 mice were used as controls (Fig. 8 and not depicted). Δ*invG* efficiently colonized the cecal lumen of mice from all four groups (Fig. 8 B). In line with earlier results, bacterial loads in the mLNs of MyD88−/− mice were ∼10-fold higher than in the control mice (Fig. 8 C) (20, 36). The bacterial loads in the mLNs of the BM chimeras were mostly determined by the genotype

of the donor. Strikingly, the BM genotype also dictated the extent of colitis. Colitis in MyD88−/− mice reconstituted with WT BM was equivalent to the colitis in WT controls. In contrast, cecal inflammation was abolished in the WT mice reconstituted with MyD88−/− BM. Thus, MyD88-dependent signaling in BM-derived cells (which includes DCs) was necessary and sufficient for triggering of colitis by Δ*invG*. In contrast, MyD88-dependent signaling in epithelial or stromal cells was not required.

Analysis of the critically involved TLR–MyD88 signaling did not yield conclusive results, as Δ*invG* could induce full-blown colitis in the absence of TLR2, TLR4, and/or TLR5 signaling (unpublished data). Our earlier work on IL-1 receptor–deficient mice had established that IL-1 receptor signaling via MyD88 was not required for Δ*invG* colitis (20). Thus, a complex and redundant network of innate immune responses involving TLR2, -4, -5, and other receptors might be involved. Future work will have to elucidate this MyD88-dependent signaling network in the BM-derived mucosal cells.

MyD88 signaling in mucosal DCs is required neither for transport nor for triggering colitis

Next, we determined whether the BM-derived cells triggering colitis via MyD88 and the CD11c+ DCs transporting Δ*invG* are the same cell type. For that purpose, we created mixed BM chimeras; after lethal γ irradiation, MyD88−/− mice were reconstituted with either 100% DTRtg BM (negative control), 50% DTRtg + 50% MyD88−/− BM (experimental group), or 50% DTRtg + 50% WT BM (positive control; Fig. 9). MyD88−/− mice and WT mice served as additional negative and positive controls. Reconstitution efficiency and mixed chimerism was controlled postmortem by FACS analysis of CD11c+ and GFP+ splenocytes and by fluorescence microscopy (unpublished data).

Every mouse was injected with DTX (depletion of DTRtg DCs) and infected for 3 d with Δ*invG* harboring the GFP tagging plasmid pM973. Colonization of the cecal lumen was similar in all experimental groups (Fig. 9 B). In line with earlier data, bacterial loads in mLN, spleens, and livers of MyD88−/− control mice were significantly higher than in the WT control mice (Fig. 9, C–E), and WT mice developed cecal inflammation, whereas MyD88−/− mice did not (Fig. 9 A). Despite the absence of inflammation, we found high numbers of intracellular (i.e., GFP-expressing) Δ*invG* in the lamina propria of the MyD88−/− mice (Fig. 9 F). Thus, the DCs of MyD88−/− mice allowed transepithelial transport of Δ*invG*, but BM-derived MyD88−/− cells failed to respond.

MyD88−/− mice reconstituted with 50% DTRtg + 50% MyD88−/− BM represented the key experimental group. It allowed for studying the role of MyD88-signaling in

A group of *n* = 5 streptomycin-pretreated C57BL/6 mice was infected with a 1:1 mixture of Δ*invG*(pDsRed) (CamR) and Δ*invG*(pM973) (AmpR), and analyzed 3 d after infection. Similar bacterial loads of Δ*invG*(pM973) and Δ*invG*(pDsRed) in the cecal lumen (F) and in mLNs (G) were determined by plating on medium containing ampicillin and chloramphenicol, respectively. (H) Numbers of DsRed+ and GFP+ bacteria per mucosal inflammatory focus. *n* = 16 inflammatory foci were analyzed in DAPI-stained serial cryosections for their content of GFP+ and DsRed+ bacteria. Foci that contained exclusively GFP+ and foci that contained only DsRed+ bacteria could be found in the same mouse (not depicted).
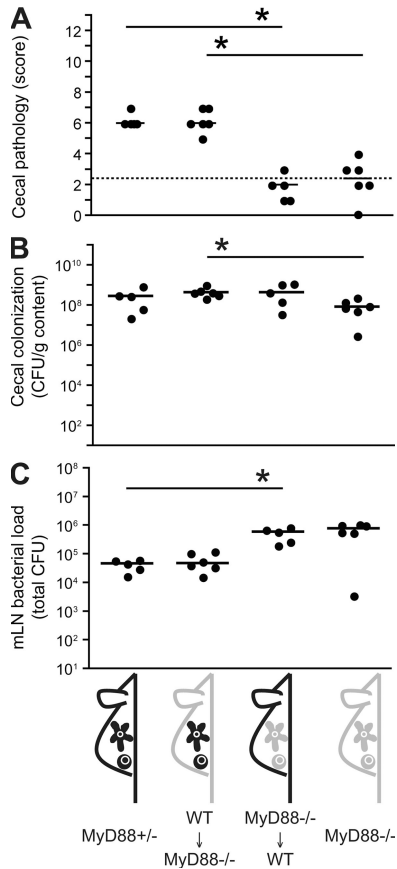
Figure 8. MyD88 signaling in BM–derived leukocytes is required and sufficient for induction of colitis by ∆invG. MyD88$^{-/-}$ mice (n = 6), MyD88$^{+/-}$ littermate controls (C57BL/6 background; n = 5), lethally irradiated MyD88$^{-/-}$ (Ly5.2) mice reconstituted with WT C57BL/6 (Ly5.1) BM (n = 6), and lethally irradiated WT C57BL/6 mice (Ly5.1) reconstituted with MyD88$^{-/-}$ (Ly5.2) BM (n = 5) were pretreated with streptomycin and infected with ∆invG (5 × 10^7 CFU by gavage). Cecal pathology scores (A), cecal luminal colonization (B), and bacterial loads in mLNs (C) were determined 3 d after infection. The y origin of every graph represents the detection limit. Dashed line, border between pathology score values observed in normal mice versus infected animals; *, statistically significant (P < 0.05).

DC-mediated bacterial translocation in more detail; after DTX treatment, bacterial translocation should rely entirely on MyD88$^{-/-}$CD11c$^+$ DCs. Once in the lamina propria, bacterial replication could occur in CD11c$^-$MyD88$^{+/+}$ leukocytes (remaining after DTX injection) and MyD88$^{-/-}$ leukocytes (which do not support cecal inflammation). Strikingly, ∆invG was translocated across the epithelium and caused a level of intestinal inflammation similar to that observed in the positive control groups (Fig. 9, A and F). Furthermore, bacterial loads in mLNs, spleens, and livers were significantly higher than in the WT control mice. This was expected for animals harboring a significant fraction of MyD88$^{-/-}$ leukocytes. In conclusion, DC-mediated translocation could occur in the absence of MyD88 signaling. In contrast, triggering of colitis required MyD88-signaling in some type of BM-derived cell, but not in DCs.

The negative control chimera (MyD88$^{-/-}$ mice reconstituted with DTR^{tg} BM) could be efficiently depleted of CD-11c^{high} cells (unpublished data). As expected for the absence of mucosal DCs, these animals did not develop colitis and had markedly reduced bacterial loads in the cecal lamina propria, mLNs, spleens, and livers (Fig. 9, C–F; compare with Fig. 3).

The positive control chimera (MyD88$^{-/-}$ mice reconstituted with 50% WT + 50% DTR^{tg} BM) displayed colitis and moderately higher bacterial loads in spleens and livers than the WT mice (Fig. 9, A, D, E). This is expected for animals with almost WT numbers of MyD88$^{+/+}$ BM-derived mucosal leukocytes.

In conclusion, the experimental group (MyD88$^{-/-}$ mice reconstituted with 50% MyD88$^{-/-}$ + 50% DTR^{tg} BM) reacted strikingly similar to the positive control chimera (MyD88$^{-/-}$ mice reconstituted with 50% WT + 50% DTR^{tg} BM). Bacterial loads in mLN, spleen, and liver, and notably the cecal inflammation, did not differ significantly. This demonstrated that MyD88$^{-/-}$ mucosal DCs are fully proficient in transepithelial transport. Yet, the MyD88-dependent inflammatory response to ∆invG is initiated subsequently by other lamina propria cells. Although these may include DCs, the inflammation is triggered efficiently in the absence of this cell type.

DISCUSSION

S. Typhimurium invades the absorptive intestinal mucosa and triggers colitis via two distinct pathways, the classical and the alternative pathway (Fig. 1). Our data demonstrate a strict DC requirement for the alternative pathway. Notably, DCs were required only during the first of the following three phases leading to acute disease: phase I, transepithelial transport; phase II, bacterial multiplication in the lamina propria; and phase III, acute MyD88-dependent inflammatory response. In phase I (0 to 18–30 h after infection), CD11c$^+$CX3CR1$^+$ DCs are essential for transepithelial transport of the bacteria from the gut lumen into the cecal lamina propria. In phase II, (18–30 to 48 h after infection) the bacteria proliferate in the lamina propria, bacterial localization shifts from CD11c$^+$CX3CR1$^+$ DCs toward predominantly CD11b$^+$CD11c$^-$CX3CR1$^-$ cells (such as lamina propria macrophages) (20), and DCs become dispensable. No overt inflammation is observed at this stage. In phase III, (48–72 h after infection), the bacterial load in the lamina propria increases to ∼10^6 CFU/g cecal tissue (estimated from Fig. 5 D), ∆invG is localized within pronounced inflammatory foci, and the acute inflammation is triggered in a MyD88-dependent fashion. The cell type responsible for initiating this MyD88-dependent inflammation is derived from the BM and is clearly distinct from the DC population mediating bacterial translocation. This defines three phases of the intestinal pathogenesis of ∆invG.

Our data demonstrate that DCs are essential for ∆invG uptake into the lamina propria. We visualized in situ that ∆invG is taken up by mucosal DCs during the first phase of the infection, and then propagates into a different host cell type (Fig. 7). However, we and others have not yet captured the exact process of epithelial traversal directly in situ, and detailed analysis is beyond the scope of this paper. We would speculate that direct
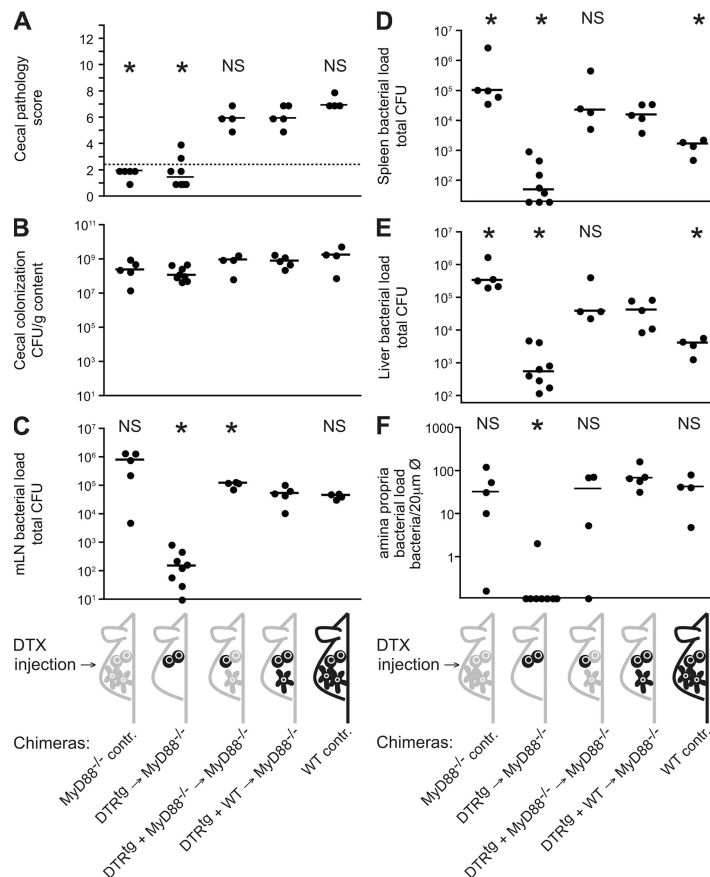
Figure 9. MyD88 signaling in mucosal DCs is not required for epithelial traversal and induction of colitis by Δ*invG*. BM chimeras and control mice were pretreated with streptomycin, injected with DTX, and infected for 3 d with Δ*invG* (pM973; 5×10^7 CFU by gavage). MyD88$^{-/-}$ controls ($n = 5$), lethally irradiated MyD88$^{-/-}$ mice reconstituted with 100% DTR^{tg} BM ($n = 8$), lethally irradiated MyD88$^{-/-}$ mice reconstituted with 50% DTR^{tg} BM and 50% MyD88$^{-/-}$ BM ($n = 4$), lethally irradiated MyD88$^{-/-}$ mice reconstituted with 50% DTR^{tg} BM and 50% WT C57BL/6 BM ($n = 5$), and C57BL/6 controls ($n = 4$) were used. Cecal pathology scores (A), cecum luminal colonization (B), and bacterial loads in mLNs (C), spleens (D), livers (E), and in the lamina propria (F) were determined 3 d after infection, representative of two independent experiments. Dashed line, border between pathology score values observed in normal mice versus. infected animals; asterisk, statistically significant difference (P < 0.05) compared with the positive control (MyD88$^{-/-}$ mice reconstituted with 50% DTR^{tg} BM and 50% WT C57BL/6 BM).

transepithelial sampling by intercalating DCs is involved. Bacterial uptake via this mechanism has been shown in vitro, and intimate association of bacteria with transepithelial DC dendrites has been visualized in the murine ileum (4–6, 28, 37). However, formation of transepithelial dendrites seems to be a too rare event in cecum and colon for unequivocal visualization (Fig. S4) (5), and is therefore difficult to assess experimentally. Notably, in our experimental system, neither streptomycin treatment (reducing the intestinal flora) nor Δ*invG* infection influenced the frequency of transepithelial DC dendrites in the ileum, which served as a control tissue (Fig. S4). The mechanism of M cell–mediated Δ*invG* translocation and subsequent DC uptake appears less likely because Δ*invG*-colitis is unaffected in Peyer's patch (PP)–deficient LTβR$^{-/-}$ mice (20). The functionality of nonfollicle-associated "villous" M cells, especially in the large intestine, is unclear (22), and we have no evidence for preferential translocation at specialized M cell–rich epithelia (unpublished data). A third possible

scenario is phagocytosis of bacteria–associated apoptotic epithelial cells by intestinal DCs (38). Thus, resolving the exact translocation mechanism remains an important objective for future research.

Do DCs also induce the inflammatory response to the Δ*invG* infection? We describe DCs that are essential for Δ*invG* translocation into the mucosa, and we have found previously that Δ*invG*-induced colitis is MyD88-dependent (20). Therefore, given the importance of DC-derived MyD88-dependent pattern recognition in mucosal innate and adaptive immunity (34, 39, 40; for review see (35, 41), we were surprised to see normal pathogen translocation and colitis induction in a mixed BM chimera with a DC-specific MyD88 deficiency. In these experiments, we clearly assigned the role of MyD88-mediated induction of inflammation to a second, CD11c$^-$ BM-derived cell type (Figs. 8 and 9). We conclude that pathogen sampling by DCs is a discrete, and MyD88-independent, step of the infection.

What is the relevance of these findings for the physiological role of DC-mediated microbial sampling in the healthy gut? The physiological mechanisms of commensal microbial sampling in the gut and the role of mucosal DCs are still controversial. In principle, recognition of all microbes seems to rely on the same, limited set of pattern recognition receptors. Thus, the intestinal innate immune system (including mucosal DCs) initially cannot discriminate between virulent *Salmonellae* (such as Δ*invG*) or commensal bacteria. This suggests that Δ*invG* and commensals are sampled from the gut lumen by the same cellular mechanism (this study) (30). Later on, however, the translocation pathways diverge, leading to killing in the case of commensals and to pathogen proliferation in the case of Δ*invG* (i.e., via TTSS-2 virulence factors) (18–20, 30). Nevertheless, the first stage of the Δ*invG* infection, MyD88-independent bacterial sampling by mucosal DCs, may also play a role in commensal sampling and maintenance of immune homeostasis.

TTSS-1⁻TTSS-2⁺ *Salmonella* strains, which are equivalent to Δ*invG*, are occasionally found on animal farms (42) and can cause human disease, as indicated by a recent human diarrheal outbreak in China (7 patients; TTSS-1⁻ *Salmonella enterica* serovar Senftenberg; Coburn, B., Q. Hu, and B.B. Finlay, personal communication). Presumably, the alternative, DC-dependent pathway of enteric *Salmonella* infection, which we describe here, is responsible for these rare cases of human infection. It should be noted that the functionality of the type III secretion systems is rarely tested in human *Salmonella* outbreaks. Therefore, the actual number of human diarrheal infections caused by TTSS-1⁻TTSS-2⁺ strains (resembling Δ*invG*) may be underestimated.

In contrast to Δ*invG*, WT *S.* Typhimurium can use two routes for intestinal invasion; the alternative pathway taken by Δ*invG* and the classical pathway involving enterocyte invasion via TTSS-1 (Fig. 1). This raises several questions. Do both pathways influence each other? Do some bacteria enter via the former and others via the latter mechanism? How does this affect progression of the acute inflammatory disease and/or the generation of an adaptive immune response? Our study paves the way for future research on the host cell factors and the bacterial virulence factors involved. These studies on a model pathogen will provide important information about the specific mechanisms allowing the intestinal immune system to handle harmless, as well as pathogenic, microbes and to generate the appropriate responses.

MATERIALS AND METHODS

Bacterial strains and growth conditions. *S.* Typhimurium SL1344 (WT Str^R) (43) and Δ*invG* (SL1344 Δ*invG*) (44) were grown in Luria-Bertani broth (0.3 M NaCl), subcultured for 4 h, and suspended in cold PBS, as previously described (45).

GFP and DsRed expression plasmids. pM973 has been previously described (20). pDsRed was generated from two PCR fragments of pDsRed-express (Clontech Laboratories, Inc.; first primer set, CGTATAAGCTTTGATTCT-GTGGATAACCGT and CGTAGGATCCTGGCGTAATCATGGT-CATAG; second primer set, CGTATGGATCCATGGCCTCCTCCGAGGA and CGTATGTCGACCTACAGGAACAGGTGGTG) cloned via HindIII,

BamHI, and SalI into pACYC184 (New England Biolabs). The resulting plasmid (pDsRed; Cam^R) expresses DsRed-express from the *lac* promoter. Δ*invG*(pDsRed) was virulent in C57BL/6 mice.

Mice. Specific pathogen–free (SPF) C57BL/6 mice (6–10 wk old) were obtained from Elevage Janvier. MyD88⁻/⁻ mice (C57BL/6 background) (46) were bred at the Biologisches Zentrallabor Zurich under SPF conditions. DTR^tg heterozygous transgenic mice (mouse line B6.FVB-Tg[Itgax-DTR/EGFP]57Lan/J) (25) and nontransgenic litter mate controls were bred by crossing DTR^tg X C57BL/6 (SPF; Elevage Janvier). These breedings, as well as C57BL/6 congenic mice carrying the Ly5.1 allele (mouse line B6.SJL-*Ptprca Pepcb*/BoyJ), transgenic B6.Tg(Itgax-EYFP) mice (expressing EYFP under CD11c control) (31), and B6.129P-*CX3CR1^tm1Litt*/J (short: CX3CR1^gfp/+) mice (47) were kept under SPF conditions in individually ventilated cages (Techniplast) at the Institute of Microbiology (Eidgenössische Technische Hochschule Zurich). Genotypes were verified via PCR typing.

For generating BM chimeras, recipients were γ irradiated (1,100 rad) and reconstituted with donor BM cells (3 × 10⁷ to 6 × 10⁷; i.v.). Reconstitution efficiency and mixed chimerism were controlled by FACS (Ly5.1/CD45.1, Ly5.2/CD45.2, CD11c, and GFP) on splenic and mLN leukocytes.

Infection experiments. *Salmonella* infections were performed in individually ventilated cages, as previously described (48). In brief, mice were pretreated by gavage with 20 mg of streptomycin. 24 h later, the mice were inoculated with 5 × 10⁷ CFU of *S.* Typhimurium by gavage or 10³ CFU by i.p. injection.

Live bacterial loads (CFU) in mLNs, spleen, and liver, as well as cecal content, were determined by plating on MacConkey agar plates (50 μg/ml streptomycin), as previously described (9).

Animal experiments were approved by the Swiss authorities (Kantonales Veterinäramt, Zürich, Switzerland; license number 201/2004) and performed according to the legal requirements.

In-vivo DC depletion. DTX was injected i.p. (100 ng/25 g body weight) (25) 18 h before and 30 h after the infection, if not stated otherwise. Depletion efficiency was controlled post mortem by FACS, immunohistology, and/or fluorescence microscopy of the cecal mucosa (number of green fluorescent DTR-GFP expressing cells ≥10-fold reduced; unpublished data).

Histopathological evaluation. 5-μm cecum mucosal cryosections were stained with hematoxylin and eosin (HE), and pathology was quantified as previously described (48). In brief, submucosal edema (0–3 score points), the number of polymorphonuclear granulocytes per high-power field in the lamina propria (0–4 score points), reduced numbers of goblet cells (0–3 score points), and epithelial damage (0–3 score points) were evaluated, and a total score of 0–13 points was obtained.

Flow cytometry. Single-cell suspensions were generated with Liberase CI/DNase (Roche) from mLNs or spleen and stained in FACS buffer (PBS, 5 mM EDTA, 1% heat-inactivated FCS [hiFCS], and 0.02% NaN₃). For large intestinal lamina propria preparations, the cecal patch was removed and the tissue was washed with ice-cold PBS, PBS (3 mM EDTA), and RPMI (Omnilab; 5% hiFCS, 1.5 mM EGTA, 1% Hepes; at room temperature for 40 min) to remove the epithelium. The tissue was chopped and digested (45 min, 37°C, RPMI with 10% hiFCS, 6 μg/ml tetracyclin, 50 μg/ml liberase, and 20 μg/ml Dnase I; Roche). The cell suspension was passed through an 18-gauge syringe 3 times, filtered through a 100-μm nylon Cell Strainer (Milian), and loaded onto a Percoll gradient (30% on 100%, iso-osmolar in PBS). After centrifugation (650 rcf for 30 min at room temperature), cells in the 30%/100% Percoll interphase were harvested and washed with FACS buffer. F_c receptors were blocked with anti-CD16/32 (F_c Block; BD Biosciences). All fluorophore-labeled monoclonal antibodies were purchased from BD Biosciences, except for the anti–Ly5.1-PE antibody (courtesy of A. Oxenius, Eidgenössische Technische Hochschule Zurich, Zurich, Switzerland). Finally, the cells were fixed in 1% paraformaldehyde (PBS) and analyzed on a FACSCalibur four-color cytometer (Becton Dickinson) and with FlowJo software (Tree Star, Inc.).

Immunohistochemistry. 5-μm-thin, acetone-fixed cryosections were stained as previously described (26) using rat antimarginal metallophilic MΦ (MOMA-1; Biomedicals) (49), rat anti-CD68 (clone FA-11; Serotec), rat anti-F4/80 (HB-198; American Type Culture Collection), rat anti-CD11b (M1/70; BMA Biomedicals AG Augst), rat anti-B220 (clone RA3-6B2; BD Biosciences), rat anti-Gr-1 (clone RB6-8C5; BD Biosciences), anti-CD3 (KTS; courtesy of R. Zinkernagel, Zürich, Switzerland), Armenian hamster anti-CD11c mAb N418 (HB-224; American Type Culture Collection), or rat anti-CD8 (YTS169) (50). Goat anti–rat Ig (Caltag Laboratories) or goat anti–Armenian hamster Ig (Jackson ImmunoResearch Laboratories) served as a secondary reagent, and HRP-coupled donkey anti–goat Ig (Jackson ImmunoResearch Laboratories; 2% normal mouse serum) served as a tertiary reagent. Slides were developed with amino-ethylcarbazol and counterstained with hemalum.

In situ detection of *S.* Typhimurium loads in the lamina propria. Cecal tissue samples were incubated overnight in PBS (4% paraformaldehyde; at 4°C for 1 h for costaining of CD11b), 8 h in PBS (20% sucrose at 4°C), and snap frozen in O.C.T. compound (Sakura). 20-μm cryosections were air dried; blocked (10% goat serum and PBS); stained with rat anti-CD11b (clone M1/70, biotinylated) or Armenian hamster anti-CD54 (clone 3E2) antibodies (both from Becton Dickinson), Streptavidin-Alexa Fluor 647 (Invitrogen), Cy3-conjugated goat anti–Armenian hamster Ig (Jackson ImmunoResearch Laboratories), DAPI (Sigma-Aldrich), and TRITC-conjugated (Sigma-Aldrich) or A647-conjugated (Fluoprobes) phalloidin; and mounted (Vectashield; Vector Laboratories). Species- and isotype-matched monoclonal antibodies (BD Biosciences) served as controls.

Δ*invG* pM973 (20) was enumerated on sections stained with anti-CD54 antibody (lamina propria staining), A647-phalloidin (brush border, cortical actin of individual gut cells), and DAPI. 10 nonserial sections per cecum (∼0.5–1% of the total cecum), or as many sections as required to collect ≥100 bacteria, were analyzed. For in situ enumeration of Δ*invG* pDsRed in CD11c-eYFP or CX3CR1^{GFP/+} transgenic mice, 15 nonserial sections (A647-phalloidin and DAPI stained) per mouse were screened.

Fluorescence imaging and image processing. Images were recorded with a microscope (Axiovert 200; Carl Zeiss, Inc.), an Ultraview confocal head (PerkinElmer), and a krypton argon laser (643-RYB-A01; Melles Griot). Infrared, red, and green fluorescence was recorded confocally, and blue fluorescence was recorded by epifluorescence microscopy. Images from Fig. 7 were recorded with a LSM510 NLO Meta system (Carl Zeiss, Inc.) using an argon laser (488 nm; green), a HeNe laser (543 nm, red; 633 nm, infrared), and a Cameleon MP two-photon laser (720 nm; DAPI). Single-layered images were transformed to the colors indicated, superimposed, and processed in Photoshop CS (Adobe); three-dimensional reconstruction and deconvolution was performed with Volocity 2.6.1. (Improvision).

Statistical analysis. Statistical analysis was performed using the exact Mann-Whitney *U* Test (Prism 4.0c). P < 0.05 (two-tailed) was considered to be statistically significant. Values were set to the minimal detectable value (10 CFU for mLN, 20 CFU for spleen, 60 CFU for liver, and 0.1/20 μm cross section for lamina propria) for samples harboring "no bacteria."

Online supplemental material. Fig. S1 shows a schematic of the DTR^{tg} transgenic model, additional data for the immunohistological analysis shown in Fig. 2 A with additional cell markers and time points, and detailed confocal microscopy analysis of DTX–induced DC cell death in DTR^{tg} CX3CR1^{GFP/+} double-transgenic mice. Fig. S2 shows FACS analysis and immunohistochemistry documenting the specificity of DC-depletion in spleens and mLNs. Fig. S3 describes a co-infection experiment with two differentially marked Δ*invG* strains applied via intestinal and systemic routes. It shows that lamina propria colonization originates from the intestinal bacterial inoculum. Fig. S4 documents the frequency of transepithelial DC dendrites in the terminal ileum and the cecum of untreated, streptomycin-pretreated, and *Salmonella*-infected CX3CR1^{GFP/+} mice. The online version of this article is available at http://www.jem.org/cgi/content/full/jem.20070633/DC1.

REFERENCES

1. Macpherson, A.J., and N.L. Harris. 2004. Interactions between commensal intestinal bacteria and the immune system. *Nat. Rev. Immunol.* 4:478–485.
2. Neutra, M.R., N.J. Mantis, A. Frey, and P.J. Giannasca. 1999. The composition and function of M cell apical membranes: implications for microbial pathogenesis. *Semin. Immunol.* 11:171–181.
3. Iwasaki, A., and B.L. Kelsall. 2001. Unique functions of CD11b+, CD8 alpha+, and double-negative Peyer's patch dendritic cells. *J. Immunol.* 166:4884–4890.
4. Chieppa, M., M. Rescigno, A.Y. Huang, and R.N. Germain. 2006. Dynamic imaging of dendritic cell extension into the small bowel lumen in response to epithelial cell TLR engagement. *J. Exp. Med.* 203:2841–2852.
5. Niess, J.H., S. Brand, X. Gu, L. Landsman, S. Jung, B.A. McCormick, J.M. Vyas, M. Boes, H.L. Ploegh, J.G. Fox, et al. 2005. CX3CR1-mediated dendritic cell access to the intestinal lumen and bacterial clearance. *Science.* 307:254–258.
6. Rescigno, M., M. Urbano, B. Valzasina, M. Francolini, G. Rotta, R. Bonasio, F. Granucci, J.P. Kraehenbuhl, and P. Ricciardi-Castagnoli. 2001. Dendritic cells express tight junction proteins and penetrate gut epithelial monolayers to sample bacteria. *Nat. Immunol.* 2:361–367.
7. Tsolis, R.M., R.A. Kingsley, S.M. Townsend, T.A. Ficht, L.G. Adams, and A.J. Baumler. 1999. Of mice, calves, and men. Comparison of the mouse typhoid model with other *Salmonella* infections. *Adv. Exp. Med. Biol.* 473:261–274.
8. Watson, P.R., S.M. Paulin, A.P. Bland, P.W. Jones, and T.S. Wallis. 1995. Characterization of intestinal invasion by *Salmonella* Typhimurium and *Salmonella* dublin and effect of a mutation in the invH gene. *Infect. Immun.* 63:2743–2754.
9. Barthel, M., S. Hapfelmeier, L. Quintanilla-Martinez, M. Kremer, M. Rohde, M. Hogardt, K. Pfeffer, H. Russmann, and W.D. Hardt. 2003. Pretreatment of mice with streptomycin provides a *Salmonella enterica* serovar Typhimurium colitis model that allows analysis of both pathogen and host. *Infect. Immun.* 71:2839–2858.
10. Stecher, B., R. Robbiani, A.W. Walker, A.M. Westendorf, M. Barthel, M. Kremer, S. Chaffron, A.J. Macpherson, J. Buer, J. Parkhill, et al. 2007. *Salmonella enterica* Serovar Typhimurium exploits inflammation to compete with the intestinal microbiota. *PLoS Biol.* 5:e244.
11. Doré, K., J. Buxton, B. Henry, F. Pollari, D. Middleton, M. Fyfe, R. Ahmed, P. Michel, A. King, C. Tinga, J. Wilson, and Multi-Provincial Salmonella Typhimurium Case-Control Study Steering Committee. 2004. Risk factors for *Salmonella* Typhimurium DT104 and non-DT104 infection: a Canadian multi-provincial case-control study. *Epidemiol. Infect.* 132:485–493.
12. Boyd, J.F. 1985. Pathology of the alimentary tract in *Salmonella* Typhimurium food poisoning. *Gut.* 26:935–944.
13. Day, D.W., B.K. Mandal, and B.C. Morson. 1978. The rectal biopsy appearances in *Salmonella* colitis. *Histopathology.* 2:117–131.
14. Raffatellu, M., R.L. Santos, D. Chessa, R.P. Wilson, S.E. Winter, C.A. Rossetti, S.D. Lawhon, H. Chu, T. Lau, C.L. Bevins, et al. 2007. The capsule encoding the viaB locus reduces interleukin-17 expression and mucosal innate responses in the bovine intestinal mucosa during infection with *Salmonella enterica* serotype Typhi. *Infect. Immun.* 75:4342–4350.

15. Zhang, S., L.G. Adams, J. Nunes, S. Khare, R.M. Tsolis, and A.J. Baumler. 2003. Secreted effector proteins of *Salmonella enterica* serotype Typhimurium elicit host-specific chemokine profiles in animal models of typhoid fever and enterocolitis. *Infect. Immun.* 71:4795–4803.

16. Hapfelmeier, S., and W.D. Hardt. 2005. A mouse model for S. Typhimurium-induced enterocolitis. *Trends Microbiol.* 13:497–503.

17. Eckmann, L. 2006. Animal models of inflammatory bowel disease: lessons from enteric infections. *Ann. N. Y. Acad. Sci.* 1072:28–38.

18. Coombes, B.K., B.A. Coburn, A.A. Potter, S. Gomis, K. Mirakhur, Y. Li, and B.B. Finlay. 2005. Analysis of the contribution of *Salmonella* pathogenicity islands 1 and 2 to enteric disease progression using a novel bovine ileal loop model and a murine model of infectious enterocolitis. *Infect. Immun.* 73:7161–7169.

19. Coburn, B., Y. Li, D. Owen, B.A. Vallance, and B.B. Finlay. 2005. *Salmonella enterica* serovar Typhimurium pathogenicity island 2 is necessary for complete virulence in a mouse model of infectious enterocolitis. *Infect. Immun.* 73:3219–3227.

20. Hapfelmeier, S., B. Stecher, M. Barthel, M. Kremer, A.J. Muller, M. Heikenwalder, T. Stallmach, M. Hensel, K. Pfeffer, S. Akira, and W.D. Hardt. 2005. The *Salmonella* pathogenicity island (SPI)-2 and SPI-1 type III secretion systems allow *Salmonella* serovar Typhimurium to trigger colitis via MyD88-dependent and MyD88-independent mechanisms. *J. Immunol.* 174:1675–1685.

21. Galan, J.E. 2001. *Salmonella* interactions with host cells: type III secretion at work. *Annu. Rev. Cell Dev. Biol.* 17:53–86.

22. Jang, M.H., M.N. Kweon, K. Iwatani, M. Yamamoto, K. Terahara, C. Sasakawa, T. Suzuki, T. Nochi, Y. Yokota, P.D. Rennert, et al. 2004. Intestinal villous M cells: an antigen entry site in the mucosal epithelium. *Proc. Natl. Acad. Sci. USA.* 101:6110–6115.

23. Bispham, J., B.N. Tripathi, P.R. Watson, and T.S. Wallis. 2001. *Salmonella* pathogenicity island 2 influences both systemic salmonellosis and *Salmonella*-induced enteritis in calves. *Infect. Immun.* 69:367–377.

24. Takeda, K., and S. Akira. 2005. Toll-like receptors in innate immunity. *Int. Immunol.* 17:1–14.

25. Jung, S., D. Unutmaz, P. Wong, G. Sano, K. De los Santos, T. Sparwasser, S. Wu, S. Vuthoori, K. Ko, F. Zavala, et al. 2002. In vivo depletion of CD11c(+) dendritic cells abrogates priming of CD8(+) T cells by exogenous cell-associated antigens. *Immunity.* 17:211–220.

26. Probst, H.C., K. Tschannen, B. Odermatt, R. Schwendener, R.M. Zinkernagel, and M. Van Den Broek. 2005. Histological analysis of CD11c-DTR/GFP mice after in vivo depletion of dendritic cells. *Clin. Exp. Immunol.* 141:398–404.

27. Salazar-Gonzalez, R.M., J.H. Niess, D.J. Zammit, R. Ravindran, A. Srinivasan, J.R. Maxwell, T. Stoklasek, R. Yadav, I.R. Williams, X. Gu, et al. 2006. CCR6-mediated dendritic cell activation of pathogen-specific T cells in Peyer's patches. *Immunity.* 24:623–632.

28. Vallon-Eberhard, A., L. Landsman, N. Yogev, B. Verrier, and S. Jung. 2006. Transepithelial pathogen uptake into the small intestinal lamina propria. *J. Immunol.* 176:2465–2469.

29. Naik, S.H., D. Metcalf, A. van Nieuwenhuijze, I. Wicks, L. Wu, M. O'Keeffe, and K. Shortman. 2006. Intrasplenic steady-state dendritic cell precursors that are distinct from monocytes. *Nat. Immunol.* 7:663–671.

30. Macpherson, A.J., and T. Uhr. 2004. Induction of protective IgA by intestinal dendritic cells carrying commensal bacteria. *Science.* 303:1662–1665.

31. Lindquist, R.L., G. Shakhar, D. Dudziak, H. Wardemann, T. Eisenreich, M.L. Dustin, and M.C. Nussenzweig. 2004. Visualizing dendritic cell networks in vivo. *Nat. Immunol.* 5:1243–1250.

32. Smythies, L.E., M. Sellers, R.H. Clements, M. Mosteller-Barnum, G. Meng, W.H. Benjamin, J.M. Orenstein, and P.D. Smith. 2005. Human intestinal macrophages display profound inflammatory anergy despite avid phagocytic and bacteriocidal activity. *J. Clin. Invest.* 115:66–75.

33. Horng, T., G.M. Barton, and R. Medzhitov. 2001. TIRAP: an adapter molecule in the Toll signaling pathway. *Nat. Immunol.* 2:835–841.

34. Kaisho, T., O. Takeuchi, T. Kawai, K. Hoshino, and S. Akira. 2001. Endotoxin-induced maturation of MyD88-deficient dendritic cells. *J. Immunol.* 166:5688–5694.

35. Hemmi, H., and S. Akira. 2005. TLR signalling and the function of dendritic cells. *Chem. Immunol. Allergy.* 86:120–135.

36. Weiss, D.S., B. Raupach, K. Takeda, S. Akira, and A. Zychlinsky. 2004. Toll-like receptors are temporally involved in host defense. *J. Immunol.* 172:4463–4469.

37. Maric, I., P.G. Holt, M.H. Perdue, and J. Bienenstock. 1996. Class II MHC antigen (Ia)-bearing dendritic cells in the epithelium of the rat intestine. *J. Immunol.* 156:1408–1414.

38. Huang, F.P., N. Platt, M. Wykes, J.R. Major, T.J. Powell, C.D. Jenkins, and G.G. MacPherson. 2000. A discrete subpopulation of dendritic cells transports apoptotic intestinal epithelial cells to T cell areas of mesenteric lymph nodes. *J. Exp. Med.* 191:435–444.

39. Uematsu, S., M.H. Jang, N. Chevrier, Z. Guo, Y. Kumagai, M. Yamamoto, H. Kato, N. Sougawa, H. Matsui, H. Kuwata, et al. 2006. Detection of pathogenic intestinal bacteria by Toll-like receptor 5 on intestinal CD11c+ lamina propria cells. *Nat. Immunol.* 7:868–874.

40. Rimoldi, M., M. Chieppa, V. Salucci, F. Avogadri, A. Sonzogni, G.M. Sampietro, A. Nespoli, G. Viale, P. Allavena, and M. Rescigno. 2005. Intestinal immune homeostasis is regulated by the crosstalk between epithelial cells and dendritic cells. *Nat. Immunol.* 6:507–514.

41. Reis e Sousa, C. 2004. Toll-like receptors and dendritic cells: for whom the bug tolls. *Semin. Immunol.* 16:27–34.

42. Rahn, K., S.A. De Grandis, R.C. Clarke, S.A. McEwen, J.E. Galan, C. Ginocchio, R. Curtiss III, and C.L. Gyles. 1992. Amplification of an invA gene sequence of *Salmonella* Typhimurium by polymerase chain reaction as a specific method of detection of Salmonella. *Mol. Cell. Probes.* 6:271–279.

43. Hoiseth, S.K., and B.A. Stocker. 1981. Aromatic-dependent *Salmonella* Typhimurium are non-virulent and effective as live vaccines. *Nature.* 291:238–239.

44. Kaniga, K., J.C. Bossio, and J.E. Galan. 1994. The *Salmonella* Typhimurium invasion genes invF and invG encode homologues of the AraC and PulD family of proteins. *Mol. Microbiol.* 13:555–568.

45. Hapfelmeier, S., K. Ehrbar, B. Stecher, M. Barthel, M. Kremer, and W.D. Hardt. 2004. Role of the *Salmonella* pathogenicity island 1 effector proteins SipA, SopB, SopE, and SopE2 in *Salmonella enterica* subspecies 1 serovar Typhimurium colitis in streptomycin-pretreated mice. *Infect. Immun.* 72:795–809.

46. Adachi, O., T. Kawai, K. Takeda, M. Matsumoto, H. Tsutsui, M. Sakagami, K. Nakanishi, and S. Akira. 1998. Targeted disruption of the MyD88 gene results in loss of IL-1- and IL-18-mediated function. *Immunity.* 9:143–150.

47. Jung, S., J. Aliberti, P. Graemmel, M.J. Sunshine, G.W. Kreutzberg, A. Sher, and D.R. Littman. 2000. Analysis of fractalkine receptor CX(3)CR1 function by targeted deletion and green fluorescent protein reporter gene insertion. *Mol. Cell. Biol.* 20:4106–4114.

48. Stecher, B., S. Hapfelmeier, C. Muller, M. Kremer, T. Stallmach, and W.D. Hardt. 2004. Flagella and chemotaxis are required for efficient induction of *Salmonella enterica* serovar Typhimurium colitis in streptomycin-pretreated mice. *Infect. Immun.* 72:4138–4150.

49. Kraal, G., and M. Janse. 1986. Marginal metallophilic cells of the mouse spleen identified by a monoclonal antibody. *Immunology.* 58:665–669.

50. Cobbold, S.P., A. Jayasuriya, A. Nash, T.D. Prospero, and H. Waldmann. 1984. Therapy with monoclonal antibodies by elimination of T-cell subsets in vivo. *Nature.* 312:548–551.